

Accepted for publication in *Ap. J.*

Direct Measurement of Neutron-Star Recoil in the Oxygen-Rich Supernova Remnant Puppis A

P. Frank Winkler

Department of Physics, Middlebury College, Middlebury, VT 05753

`winkler@middlebury.edu`

and

Robert Petre

NASA Goddard Space Flight Center, Greenbelt, MD

`robert.petre-1@nasa.gov`

ABSTRACT

A sequence of three *Chandra* X-ray Observatory High Resolution Camera images taken over a span of five years reveals arc-second-scale displacement of RX J0822–4300, the stellar remnant (presumably a neutron star) near the center of the Puppis A supernova remnant. We measure its proper motion to be 0.165 ± 0.025 arcsec yr $^{-1}$ toward the west-southwest. At a distance of 2 kpc, this corresponds to a transverse space velocity of ~ 1600 km s $^{-1}$. The space velocity is consistent with the explosion center inferred from proper motions of the oxygen-rich optical filaments, and confirms the idea that Puppis A resulted from an asymmetric explosion accompanied by a kick that imparted roughly 3×10^{49} ergs of kinetic energy (some 3 percent of the kinetic energy for a typical supernova) to the stellar remnant. We discuss constraints on core-collapse supernova models that have been proposed to explain neutron star kick velocities.

Subject headings: ISM: individual (Puppis A) — X-rays: individual (RX J0822–4300) — stars: neutron — (stars:) supernovae: general — (ISM:) supernova remnants — astrometry

1. Introduction

There has long been broad consensus that core-collapse supernovae—the explosions of massive progenitors that produce Types II, Ib, and Ic events at least—leave behind a compact stellar remnant: either a neutron star or a black hole. Early on, this model was marred by the paucity of observed compact objects associated with supernova remnants (SNRs). The discovery in recent years of numerous compact X-ray sources associated with SNRs, especially with the oxygen-rich SNRs that are presumably the young remnants of core-collapse SNe, has removed this blemish (e.g. Manchester 2001, for a recent review). Compact stellar remnants have been identified near the centers of all three of the known oxygen-rich SNRs in the Galaxy—Cas A (Tananbaum 1999; Chakrabarty et al. 2001), Puppis A (Petre et al. 1996), and most recently G292.0+1.8 (Hughes et al. 2001; Camilo et al. 2002)—plus 0540–69.3 in the LMC (Seward et al. 1984).

There is also growing evidence, both observational and theoretical, that the explosions of core-collapse SNe are asymmetric. In young, oxygen-rich SNRs, whose fast filaments provide the best opportunities for observing ejecta from the cores of massive SNe, anisotropies appear to be typical: e.g., Cas A (Lawrence et al. 1995; Reed et al. 1995; Fesen 2001; Hwang et al. 2000, 2004), and the LMC remnants N132D (Morse et al. 1995), and 0540–69.3 (Kirshner et al. 1989), in addition to Puppis A (Winkler & Kirshner 1985). Furthermore, two-dimensional models for core-collapse SNe show instabilities just prior to collapse that produce asymmetries in the ejecta distribution (e.g., Burrows et al. 1995).

Simple conservation of momentum requires that if the explosion of a progenitor star expels the ejecta preferentially in one direction, the compact core must recoil in the opposite direction. By measuring the displacements of young pulsars from the apparent centers of their associated SNR shells and using the pulsar spin-down periods as age estimates, Caraveo (1993) and Frail et al. (1994) inferred that pulsars are typically born with transverse velocities of 500 km s^{-1} , and that velocities $\gtrsim 2000 \text{ km s}^{-1}$ may occur. Direct radio and optical measurements have found transverse velocities ranging from 60 km s^{-1} (for Vela – Dodson et al. 2003) to 240 km s^{-1} (for PSR B1951+32 in CTB 80 – Migliazzo et al. 2002).

Here we report measurement of the recoil of RX J0822–4300, the presumed neutron star near the center of Puppis A, obtained through images taken at three epochs spanning 5 years from the High Resolution Camera (HRC) on the *Chandra* X-ray Observatory. Past optical studies of the most prominent ejecta-dominated filaments show that they are concentrated in the northeast quadrant of the remnant, and that their motions are northward and eastward, consistent with undecelerated expansion from a common center (Winkler & Kirshner 1985; Winkler et al. 1988). The present measurement of the stellar remnant’s rapid motion to the west-southwest completes a picture of asymmetric ejecta and neutron star recoil resulting

from a core-collapse supernova.

As the original version of this paper was nearing completion, we became aware of a paper by Hui & Becker (2006a, henceforth HB06) that presents a similar analysis based on two of the three *Chandra* observations used here. While the HB06 result is qualitatively similar to our own, our analysis leads to a more precise measurement and a significantly higher velocity for RX J0822–4300. We compare their methods with our own in §3.5.

2. Observations

The compact X-ray source near the center of Puppis A, RX J0822–4300, was observed with the HRC-I in December 1999 (OBSID 749), and again with the HRC-S in January 2001 (OBSID 1851). We repeated the earlier of these previous observations, using the HRC-I, on 25 April, 2005 (OBSID 4612). For all three observations, RX J0822–4300 was placed essentially on-axis for optimum spatial resolution. The observational details are summarized in Table 1.

At the ~ 2 kpc distance of Puppis A, a transverse velocity of 1000 km s^{-1} would give a proper motion of only $\sim 0\rlap{.}''1 \text{ yr}^{-1}$. Given *Chandra*'s uncertainty of $\sim 0\rlap{.}''5$ in absolute aspect, measurement of the motion over a baseline of a few years is a challenge. By great good luck, there are two additional point sources quite close to RX J0822–4300, almost optimally situated for a proper motion study. The closer, which we refer to as Star A, is located $2\rlap{.}7$ to the southwest of the stellar remnant; the other, Star B, is $5\rlap{.}4$ to the northeast. Both coincide with $V \sim 13\text{--}14$ mag stars included in the UCAC2 astrometric catalog (Zacharias et al. 2003), with precisely measured (within 15–24 mas) positions and proper motions. Therefore, it is possible to use these stars as fiducial sources to provide a precise absolute coordinate system for the image at each epoch.

For each of the three HRC images, we first identified the sources and measured their positions using the standard WAVDETECT routine in the Chandra Interactive Analysis of Observations (CIAO) software package (version 3.3). RX J0822–4300 and both fiducial stars were detected with high signal-to-noise ($> 5\sigma$) in all three observations, with positions within $0\rlap{.}''6$ of the UCAC2 catalog positions. There can be no doubt that the association of the X-ray sources with the UCAC2 stars is correct. In addition, there is another, very faint, X-ray source in the field at a position only $2\rlap{.}0$ from RX J0822–4300 and coincident within $0\rlap{.}''5$ with a third UCAC2 star (Star C). This source was detected at the $\sim 3\sigma$ level in the first two *Chandra* observations (1999 and 2001), but the detection was extremely marginal (~ 5 counts $\lesssim 2\sigma$) in the 2005 observation. In order to maintain consistency, we did not use

it for the astrometry in any of the images.

Relevant data for all three stars, extracted from the UCAC2 catalog, appear in Table 2. All three also appear in the 2MASS catalog (Cutri et al. 2003) at positions consistent with those in the UCAC2 but with lower precision. In Figs. 1 and 2, respectively, we show the central region of an image from the 2005 HRC-I observation with the sources marked, and the identical field in an optical image taken with the CTIO 0.9 m telescope through a narrow-band red filter (CWL 6852 Å, FWHM 95 Å).

3. Precise Astrometry and Proper Motion Measurement

As a preface to this section, we note that the proper motion of RX J0822–4300 (which we refer to more succinctly as the neutron star, NS) is apparent in the data. Simple comparison between images based on the original level-2 event files with the nominal aspect shows a displacement of order 1" west, and slightly south, from the Dec 1999 HRC-I observation to the one in April 2005. The difference is noticeable by blinking the two images, and is even more apparent when one scales the images by the exposure time and subtracts one from the next.

The absolute aspect of *Chandra* HRC images may be subject to uncertainty of order 0".5, however, so we have gone to considerable effort to achieve the highest accuracy possible in the astrometry, based on the fiducial stars A and B. We discuss below two techniques, the first a simple translation from one epoch to the other (applicable for the HRC-I images only), and the second involving transformation of all three images to an absolute world coordinate system based on the optical positions for the fiducial stars. Both techniques begin with precise measurement of the X-ray positions of the NS and stars A and B on each HRC image, discussed in §3.1. The subsequent sections describe the two transformation techniques and proper-motion measurements. Since the measurement involves pushing HRC astrometry to its limits, we describe these steps in some detail.

3.1. Nominal X-ray Positions

For the final analysis we reprocessed the *Chandra* level-1 event files to incorporate the latest degapping and tap-ringing corrections. We then used the *Chandra* ray-tracing and simulation (ChaRT/MARX) routines to generate off-axis point-spread functions (PSFs) appropriate for each of the three sources at each epoch, following the ChaRT threads “Using MARX to Create an Event File” and “Creating an Image of the PSF,” and normalized these

to match the observed counts in each image. We then followed the CIAO/Sherpa thread “Using a PSF Image as the Convolution Kernel” to obtain the best-fit position for each source. This procedure convolves the appropriate PSF with a source model, and varies the model parameters to achieve the best match to the data. For the NS and star A we used the original (unbinned) data with a scale of $0.^{\prime\prime}1318$ pixel $^{-1}$, but for star B we binned the data (and the matching PSF) 2×2 .

As a source model we used a narrow Gaussian with FWHM fixed at 1 pixel $\simeq 0.^{\prime\prime}13$ (\ll the PSF width, even for a near on-axis source),¹ and varied four parameters: x and y position (RA and Dec, respectively), source strength, and (constant) background level. Convolving this model with the appropriate PSF matches the original data well in all cases. We also experimented with varying the width of the Gaussian, and found that the fits are insensitive to the choice of FWHM as long as it is $\lesssim 3$ pixels. There is no evidence for a finite extent to the NS source (nor for either of the stellar sources). In Fig. 3 we show an example of one of the position fits, for star A at the 2005 epoch.

The results of the position fits for all three sources (based on the nominal aspect solution) at all three epochs are given in Table 3. All are based on fits like the one illustrated in Fig. 3. The uncertainties represent the $1-\sigma$ (68% confidence) limits for the source position along the x and y axes. To obtain these, we used Sherpa to calculate the Cash (1979) statistic over a grid and used an increment of 2.3 above the minimum as the estimate of the $1-\sigma$ confidence limit for a model with two “interesting” parameters (Press et al. 1992). An example of a Cash-statistic contour plot resulting from this procedure is shown in Fig. 3, panel (d). We note that the contours are not circular; when projecting along a different axis (as we do in §3.4) we used the actual values appropriate for that direction, as measured graphically on these plots.

3.2. Method 1: Simple Translations

The simplest approach to measuring the NS proper motion is a two-dimensional translation of the image from the second epoch relative to the first, based on the fiducial stars. If all aspects of the instrument and the data train are identical, this ought to bring the fiducial stars into alignment. But translation alone is only modestly successful in aligning stars A

¹The alternative of a model using a true point source leads to similar results for the fitted position, but (as currently implemented in Sherpa) fails to produce maps of confidence contours with sufficient resolution to give precise uncertainties. An example of such a map for the narrow Gaussian model we actually used is in panel (d) of Fig. 3.

and B in the pair of images from the two HRC-I epochs. Even after correcting for the (small) proper motions of the stars (taken from the UCAC2) between epochs, we find shifts for stars A and B that differ by $(0''.95 \pm 0''.31, -0''.71 \pm 0''.42)$ in x and y , respectively. An average shift weighted inversely as the variance is dominated by the shift for the more nearly on-axis star A, and leads to a change in the NS position of $(-0''.71 \pm 0''.12, -0''.25 \pm 0.20)$ in RA and Dec, respectively, from epoch 1998.98 to 2005.32, or proper motion $0''.141 \pm 0''.024 \text{ yr}^{-1}$ at an angle of $20^\circ \pm 14^\circ$ south of due west. The uncertainties are purely formal, based on uncertainties in the position fits for stars A and B, the (much smaller) uncertainties in the proper motions for the optical stars, and the (negligible) uncertainties in the position fit for the NS at the two epochs (all as given in Table 3). We did not attempt a similar pure translation between the HRC-S and HRC-I images, since there is a known small rotational offset between the HRC-S and HRC-I, and possibly other small systematic effects as well (R. Kraft, private communication).

3.3. Method 2: Transformation to an Absolute Frame

A more sophisticated technique follows precise measurement of the X-ray positions of the NS and Stars A and B on each HRC image (§3.1) with transformation of both HRC images to a common *absolute* world coordinate system (WCS) based on the catalogued optical positions for stars A and B. Then the NS position at each epoch, its motion between epochs, and uncertainties in these quantities may be determined from the transformations. We assume that the “true” positions for stars A and B are those for the optical stars given by the UCAC2, corrected for proper motion to the appropriate epoch. These are also given in Table 3. We then calculate the transformation so that the measured X-ray positions will exactly match the optical ones at each epoch.

We assume a linear transformation that involves four parameters: translations in x and y (t_x and t_y), rotation through an angle θ , and a uniform change in scale by a factor r . With only two fiducial points it is straightforward to calculate a unique transformation analytically. The transformation parameters are determined from (x_A, y_A) , (x_B, y_B) , the x and y positions for stars A and B as measured in an HRC image, and (x'_A, y'_A) , (x'_B, y'_B) , the reference positions from the UCAC2 at the same epoch. The transformation is calculated by

$$\begin{pmatrix} -y_A & x_A & 1 & 0 \\ x_A & y_A & 0 & 1 \\ -y_B & x_B & 1 & 0 \\ x_B & y_B & 0 & 1 \end{pmatrix} \begin{pmatrix} p \\ q \\ t_x \\ t_y \end{pmatrix} = \begin{pmatrix} x'_A \\ y'_A \\ x'_B \\ y'_B \end{pmatrix}, \quad (1)$$

where $p = r \sin \theta$ and $q = r \cos \theta$. Inverting the matrix leads to the transformation parameters t_x , t_y , r , θ , which we then apply to the position of the NS measured on the *Chandra* image to find its corrected position at that epoch,

$$\begin{pmatrix} x'_{NS} \\ y'_{NS} \end{pmatrix} = \begin{pmatrix} q & -p \\ p & q \end{pmatrix} \begin{pmatrix} x_{NS} \\ y_{NS} \end{pmatrix} + \begin{pmatrix} t_x \\ t_y \end{pmatrix}. \quad (2)$$

The results of our transformation analysis indicate corrections to the nominal aspect that are small, but significant at the sub-arcsecond level. The stretch factors r required to scale from the original frame to the absolute one are 1.0022(6), 1.0033(3), and 1.0002(2) for data from the 1999 HRC-I, 2001 HRC-S, and 2005 HRC-I observations, respectively, where the number in parentheses represents the uncertainty in the final digit. The rotation angles (in the same order) are $-0^\circ 01(4)$, $+0^\circ 12(2)$, and $0.00(1)$. The translations in x and y are all $\lesssim 0''.5$.

The adjusted position for the NS at each epoch and its proper motion between epochs are given in Table 4. The two pairs of measurements with baselines longer than 4 years—OBSIDs 749 vs. 4612 (5.34 yr), OBSIDs 1851 vs. 4612 (4.25 yr)—both yield results that are very similar to one another and to the measurement translation-only analysis for the 749-4612 pair (§3.2): a displacement corresponding to a proper motion of $\sim 0''.16 \text{ yr}^{-1}$ in a direction 15° – 30° south of west. The total displacement from 1999 December until 2005 April is $0''.75$ based on pure translation, or $0''.99$ based on the more general transformation. From 2001 January until 2005 April the displacement is $0''.72$. For our overall measurement we adopt the unweighted mean of all three measurements: $0''.165 \pm 0''.025 \text{ yr}^{-1}$ at position angle $248^\circ \pm 14^\circ$. Whatever the technique used, the statistical uncertainty is dominated by uncertainty in measuring the X-ray positions for the reference stars. We discuss this further in §3.4.

In Fig. 4 we show a difference image between the December 1999 and April 2005 exposures (registered and scaled by the exposure time). The only strong feature is at the position of the stellar remnant. The inset shows a small region surrounding the stellar remnant from Figs. 1 and 4. The evidence for movement of RX J0822-4300 is unequivocal.

3.4. Uncertainty Estimate, and a Simplification

The variance in x'_{NS} and y'_{NS} may be calculated by combining in quadrature the contributions from each of the 10 measured quantities, x_A , y_A , x_B , y_B , x'_A , y'_A , x'_B , y'_B , x_{NS} , and

y_{NS} , by

$$\sigma_{x'_{NS}}^2 = \left(\frac{\partial x'_{NS}}{\partial x_A} \right)^2 \sigma_{x_A}^2 + \left(\frac{\partial x'_{NS}}{\partial y_A} \right)^2 \sigma_{y_A}^2 + \cdots + \left(\frac{\partial x'_{NS}}{\partial y_{NS}} \right)^2 \sigma_{y_{NS}}^2. \quad (3)$$

For finding the *magnitude* of the proper motion, this tedious calculation can be considerably simplified by a very fortuitous accident: the NS position lies not far off the line joining stars A and B, and furthermore the direction of its motion is nearly parallel to this line. We can thus work in a coordinate system (u, v) that is rotated by 30.5° clockwise with respect to the (x, y) system, so that the u axis runs parallel to the line from B to A.² The original two-dimensional problem may then be approximated by a one-dimensional one: finding the position of an intermediate point along an elastic band that we allow to stretch uniformly between end points at known locations. Based on only five measured quantities—the u coordinates for the three X-ray sources, which we denote as a , b , and n for stars A, B, and the NS, respectively, and the corresponding optical coordinates for stars A and B, denoted as a' and b' —we can calculate n' , the true position for the NS along the u axis, along with its uncertainty $\sigma_{n'}$.

In this one-dimensional approximation, the transformation from the measured X-ray position u at any epoch to the reference (optical) position is given simply by $u' = ru + t$, where r is a stretch factor and t a translation. Writing the transformation for the reference points a and b , we immediately find

$$r = \frac{b' - a'}{b - a}, \quad t = a' - \frac{b' - a'}{b - a}a, \quad (4)$$

and thus n' is

$$n' = a' + \frac{b' - a'}{b - a} (n - a). \quad (5)$$

In the usual manner for obtaining the variance in a quantity that depends on several independent variables,

$$\sigma_{n'}^2 = \left(\frac{\partial n'}{\partial a} \right)^2 \sigma_a^2 + \left(\frac{\partial n'}{\partial b} \right)^2 \sigma_b^2 + \left(\frac{\partial n'}{\partial n} \right)^2 \sigma_n^2 + \left(\frac{\partial n'}{\partial a'} \right)^2 \sigma_{a'}^2 + \left(\frac{\partial n'}{\partial b'} \right)^2 \sigma_{b'}^2. \quad (6)$$

Straightforward calculation of the partial derivatives gives results such as

$$\frac{\partial n'}{\partial a} = \frac{(n - b)(b' - a')}{(b - a)^2} = r \frac{(n - b)}{(b - a)} \approx \frac{(n - b)}{(b - a)}, \quad (7)$$

²While this line will be in slightly different directions at the different epochs, due to proper motions of A and B, we have used the orientation at the 2005 epoch for all. Proper motions of the reference stars lead to slightly different (u, v) coordinates for each at the different epochs, but the contribution of differences in v to the scale factor are negligible.

where the final approximation utilizes the fact that the stretch factor r is very nearly 1. With similar approximations for the other derivatives, (7) becomes

$$\sigma_{n'}^2 \approx \left(\frac{n-b}{b-a} \right)^2 (\sigma_a^2 + \sigma_{a'}^2) + \left(\frac{n-a}{b-a} \right)^2 (\sigma_b^2 + \sigma_{b'}^2) + \sigma_n^2. \quad (8)$$

The individual uncertainties in Table 4 are calculated in this way and include the formal uncertainties in fits to the X-ray positions for stars A and B and for RX J0822–4300, and also the (smaller) position uncertainties from the UCAC2 catalog, for both epochs. We have included proper-motion uncertainties from the UCAC2, so the overall position uncertainty for the astrometric stars increases with time since the 2000.0 reference epoch. However, uncertainties in the X-ray source positions still dominate at all three epochs. Not surprisingly, the statistical uncertainties in all three proper-motion determinations are comparable. For our final result, we have taken a conservative approach: an unweighted average of the three measurements, with an uncertainty comparable to that of any of the individual ones and large enough to embrace them all.

3.5. Comparison with Hui & Becker (2006a)

In their analysis, HB06 have obtained a qualitatively similar but smaller and more uncertain value for the proper motion: $0.^{\circ}104 \pm 0.040 \text{ yr}^{-1}$ at position angle $240^\circ \pm 28^\circ$. Their analysis differs from our own in several respects: (1) They used only the two HRC-I observations, while we have also included the 2001 observation with the HRC-S. (2) HB06 used only the closer of the two stars in the field (star A in our nomenclature; star B in theirs) as an astrometric reference, while we used both. (3) HB06 based their position fits on PSF’s interpolated from the library in CALDB, while ours are based on PSF’s we generated specifically for each source and observation using ChaRT and MARX. (The CIAO thread “Why use ChaRT instead of the PSF libraries?” explicitly discusses this difference.) (4) HB06 took the absolute position of their reference star from the 2MASS catalog, whereas we used the somewhat more precise ones from UCAC2 that also include proper-motion corrections. Despite these differences, the fact that independent analyses carried out by different groups lead to results that are *qualitatively* similar—the neutron star recoiling to the west-southwest with high velocity—further supports the robustness of the result. However, there are significant quantitative differences: HB06a found $\mu = 0.^{\circ}104 \pm 0.040 \text{ yr}^{-1}$ vs. our measurement of $0.^{\circ}165 \pm 0.025 \text{ yr}^{-1}$. We discuss some implications of such a high proper motion and the implied transverse velocity in the next two sections.

4. Space Velocity and Kinematics

The most recent estimate for the distance to Puppis A is by Reynoso et al. (1995), who found 2.2 ± 0.3 kpc, based on the velocity of H I absorption features. An independent estimate is 1.8 ± 0.5 kpc, based on a possible association with Vela OB1 (Sakhibov & Smirnov 1983). For simplicity, we calculate the space velocity scaled to a distance $d_2 \equiv d/2$ kpc. The measured proper motion of $0''.165 \pm 0.025$ yr $^{-1}$ corresponds to a transverse space velocity of $1570 \pm 240 d_2$ km s $^{-1}$. The high proper motion confirms the general picture of an asymmetric explosion of the Puppis A progenitor, accompanied by a violent kick to the stellar remnant; a neutron star space velocity exceeding ~ 100 km s $^{-1}$ cannot be produced by the break up of a binary system by a supernova.

Petre et al. (1996) predicted just this sort of motion for RX J0822-4300 based on its position 6' west-southwest of the expansion center for the oxygen knots measured by Winkler et al. (1988). For an age of 3700 yr, also determined by the knot kinematics, the expected transverse velocity is $980 d_2$ km s $^{-1}$. As shown in Fig. 5, extrapolation backwards from RX J0822-4300 along the vector representing the measured proper motion almost grazes the 90% confidence contour for the explosion center. The present measurement provides strong qualitative confirmation for the picture of a recoiling neutron star as laid out by Petre et al. (1996), but it appears that the actual velocity is $\sim 50\%$ higher than they predicted. This suggests that the Puppis A remnant is somewhat younger than 3700 yr, and/or that the true expansion center is somewhat west and south of the one found by Winkler et al. (1988).

How asymmetric was the explosion? Given a velocity of $1570 d_2$ km s $^{-1}$ and a nominal neutron star mass of $1.4 M_\odot$, the kinetic energy of associated with the compact star is $\sim 3 \times 10^{49} d_2^2$ ergs. This represents 3% of the total kinetic energy of 10^{51} ergs produced by a canonical supernova explosion. Conservation of momentum requires that the net momentum of material ejected in the opposite direction is $1.4 M_\odot \times 1570$ km s $^{-1} \sim 4 \times 10^{41}$ g cm s $^{-1}$.

Overall the Puppis A remnant looks reasonably symmetric in X-rays after the northeast-erly gradient in the density of the ambient medium is taken into account. Any asymmetries associated with the forward shock have long been submerged by asymmetries in the ISM. Oxygen is the most prominent ejecta species: the *Einstein* FPCS detected a substantial overabundance of highly ionized oxygen at $\sim 2 \times 10^6$ K. Assuming the oxygen is uniformly dispersed throughout the remnant, Canizares & Winkler (1981) estimated a total oxygen mass of $> 3 M_\odot$, from which they inferred a progenitor mass of $> 25 M_\odot$. Subsequent X-ray spectral imaging has not revealed any asymmetry in oxygen or any other ejecta species (Tamura et al. 1994). The only manifestation of asymmetry is the array of fast moving knots, composed almost entirely of warm ([O III]-emitting) oxygen and neon (Winkler & Kirshner 1985; Winkler et al. 1988).

It is possible to estimate whether sufficient mass is contained in these knots to balance the momentum. Winkler et al. (1988) give 0.1 pc and 200 O atoms cm^{-3} as the typical knot size and density, for a mass $\sim 0.04M_\odot$. The proper motions for the 11 measured knots correspond to 1,000-2,500 km s^{-1} at 2 kpc. For a typical velocity component opposite the direction of the stellar remnant of 1,500 km s^{-1} , the corresponding momentum per knot is $\sim 1.2 \times 10^{40} \text{ g cm s}^{-1}$. Thus ~ 30 such knots are needed to offset the momentum of RX J0822–4300. Fig. 5 suggests the existence of this number of knots is reasonable.

5. Discussion

The nature of RX J0822–4300 is not well understood. Like most other objects lumped into the “central compact object” class, it is detected only in X-rays and shows no strong long- or short-term temporal variability. Hui & Becker (2006b) find a candidate period of ~ 0.22 s, with a 5 ± 1 percent pulsed fraction.³ Its X-ray spectrum and flux are consistent with thermal emission from a neutron star surface. Pavlov et al. (2002) find acceptable fits using either a black body with $kT \sim 0.4$ keV and an emitting radius $R \sim 1.4$ km, or a hydrogen atmosphere model with $kT_{eff}^\infty \sim 0.17$ keV, an emitting radius $R_\infty \sim 10$ km, and surface magnetic field strength $B \gtrsim 6 \times 10^{12}$ G; Hui & Becker (2006b) prefer a two black body fit with temperatures and effective radii $T_1 = 2.6 \times 10^6$ K, $T_2 = 5.0 \times 10^6$ K, $R_1 = 3.3$ km, and $R_2 = 0.75$ km. Hui & Becker (2006b) place an upper limit of 2.9×10^{-13} ergs $\text{cm}^{-2} \text{ s}^{-1}$ on the 0.5 - 10.0 keV X-ray flux from an associated wind nebula. An extremely stringent constraint has been placed on the radio luminosity of a wind nebula, three orders of magnitude below what would be expected if the stellar remnant were an energetic young pulsar (Gaensler et al. 2000). The resulting stringent radio limit on \dot{E} suggests a high magnetic field ($B > 6.4 \times 10^{13}$ G), which in turn invites comparison of this object with AXPs and SGRs. Such a comparison is premature, however, given the different spectral and temporal properties of RX J0822–4300. Velocity is not a discriminator, as AXPs and SGRs show a large range of inferred transverse velocities, from $< 100 \text{ km s}^{-1}$ to $\sim 2900(3 \text{ kyr}/t) \text{ km s}^{-1}$ (Gaensler 2000).

The object most similar to RX J0822–4300 is the central stellar remnant in Cas A. Cas A is thought to be the result of the core-collapse explosion of a comparably massive star (Willingale et al. 2003), with oxygen its most abundant nucleosynthesis product. Its stellar remnant has similar spectral properties to the one in Puppis A, though the one in Cas A is slightly hotter, as should be the case for a neutron star one-tenth the age (Pavlov et al.

³The 75 ms period once-proposed for RX J0822–4300 has not withstood further scrutiny (Pavlov et al. 2002; Hui & Becker 2006b).

2002). It too shows no evidence for either a wind nebula or strong temporal variability.⁴ Its transverse velocity is inferred to be 330 km s^{-1} for a distance of 3.4 kpc (Thorstensen et al. 2001), perpendicular to the most pronounced asymmetry axis in the remnant, defined by the “jet” and “counter jet” (Hwang et al. 2004).

The most challenging problem is to explain how neutron stars can have recoil velocities as high as we have measured for RX J0822–4300. Numerous mechanisms have been proposed to provide kicks to nascent neutron stars during a supernova explosion. Generally speaking, these fall into three broad categories: electromagnetically driven, neutrino/magnetic-field driven, and hydrodynamically driven. A review of the physics of each can be found in Lai (2001). Briefly, in the electromagnetically driven mechanism, radiation from an off-centered rotating magnetic dipole imparts a gradual acceleration to the neutron star along its spin axis. In the neutrino/magnetic-field driven mechanism, the kick is produced by asymmetric neutrino emission arising in a strong magnetic field. The hydrodynamically driven mechanism relies on asymmetric matter ejection resulting from hydrodynamic instabilities during the explosion. The first two mechanisms lead naturally to alignment of the kick direction close to the neutron star spin axis. Electromagnetically driven kicks can generate a spin-aligned kick of $1,000 \text{ km s}^{-1}$, but require millisecond spin periods do to so. Neutrino/magnetic-field driven kick models do not produce velocities higher than $\sim 250 \text{ km s}^{-1}$ and require magnetic fields in excess of 10^{15} G . Both these mechanisms seem unlikely candidates for the origin of RX J0822–4300.

Hydrodynamically driven shocks can in principle also provide kick velocities in excess of $1,000 \text{ km s}^{-1}$ and do not require spin-kick alignment. (Burrows & Hayes 1996; Burrows et al. 2006, 2007; Scheck et al. 2004, 2006). However, a spin-kick alignment can occur during a hydrodynamically driven kick if rotation is dynamically important for the core collapse and explosion (which in turn requires the initial spin period to be less than 1 ms). Alternatively, alignment can occur hydrodynamically from rotational averaging of the transverse momentum from small thrusts, provided the kick duration is substantially longer than the rotation period of the proto-neutron star (Spruit & Phinney 1998). Spin-kick alignment or near-alignment seems to be a common trait of isolated pulsars and neutron stars associated with pulsar wind nebulae (Ng & Romani 2004; Johnston et al. 2005; Wang et al. 2006), but appears to be less common in neutron stars in binary systems (Wang et al. 2006).

Evidence regarding spin-kick alignment of RX J0822–4300 is mixed. The strongest supporting evidence is the existence of of a bipolar cavity observed in H I centered on the

⁴As for RX J0822–4300, the claimed periodicity of 12 ms of the Cas A source has not been confirmed (Murray et al. 2002).

star and oriented approximately along the direction of motion (Reynoso et al. 2003). These are postulated to arise from oppositely directed jets; they have swept out approximately $2 M_{\odot}$ of material. The absence of readily detectable pulsations argues against alignment: if the system were aligned, the apparent space velocity vector, largely in the plane of the sky, provides an ideal viewing geometry for detecting pulsations. Alternatively, the marginal detection requires alignment not only of the spin and kick directions, but also the magnetic field vector.

Independent of the spin-kick alignment question, the high transverse velocity of RX J0822–4300 together with its other properties challenge explosion models that produce neutron-star kicks. The high magnetic field required for the electromagnetically-driven mechanism is consistent with the absence of a wind nebula, but the absence of a period in the 6–12 s range typical of magnetars argues against such a mechanism. Electromagnetically driven kicks are generally viewed as unlikely because these require very fast (ms) spin periods, which are not associated with isolated pulsars. Kick mechanisms driven by neutrinos may be ruled out by the momentum balance between RX J0822–4300 and the oxygen knots as well as by the high velocity. The presence of these knots, along with the lack of pulsations and the analogy with Cas A, all favor a non-aligned kick of hydrodynamic origin.

Recent SN explosion modeling by Burrows et al. (2007) makes two important predictions. This model posits a mechanism for core-collapse SNe relying on acoustic power generated in the inner core. The recoil mechanism is hydrodynamical, due either to acoustic power or an asymmetric neutrino flux. First, their model provides an estimate of the kick velocity: $v_k \sim 1000 E/(10^{51} \text{ ergs}) \sin \alpha \text{ km s}^{-1}$, where E represents the explosion energy, and $\sin \alpha$ parameterizes the anisotropy of the explosion. This expression predicts a correlation between explosion energy and neutron star recoil velocity. Even for the most extreme anisotropy, $\sin \alpha \sim 1$, this model suggests that the explosion producing Puppis A must have been more energetic than the canonical 10^{51} ergs, and could have been considerably more so. It is currently thought that the explosion producing Cas A had energy $2\text{--}4 \times 10^{51}$ ergs (Laming et al. 2006); thus by analogy, a similar explosion energy might be expected for Puppis A. A higher explosion energy offers the benefit (for this model) of reducing the energy fraction that must be channeled into the kick.

A second prediction of the Burrows et al. (2007) model is that the proto-neutron star and a compensating amount of inner ejecta are expelled in opposite directions. The inner ejecta in core-collapse SNe are thought to be predominantly iron. The oxygen knots originate in an outer, hydrostatic burning layer, and move much more slowly than the initial velocity of material ejected from nearer the core. There is no evidence for excess Fe opposite the stellar direction of motion, however, or anywhere else in Puppis A. If fast Fe ejecta are

present towards the east-northeast (up an ambient density gradient), one would expect these to become visible through interaction with the medium. The only apparent ejecta concentration is a region of enhanced Si to the north-northeast of RX J0822–4300, and not in line with its motion (Hwang et al. 2007). If the O knots are the only manifestation of an explosion asymmetry, it is not apparent how the momentum of the inner ejecta could be efficiently transferred to them.

6. Conclusions

As a summary, we may highlight the following points: (1) A precise position for RX J0822–4300, the presumed neutron star, has been measured from three independent *Chandra* HRC observations spread over a baseline of over five years. Comparison among these yields a proper motion of $0''.165 \pm 0''.025 \text{ yr}^{-1}$ at position angle $248^\circ \pm 14^\circ$. The uncertainty is dominated by the precision of position fits for two fiducial stellar X-ray sources used in the analysis.

(2) This motion implies a transverse velocity of $1570 \pm 240 (d/2 \text{ kpc}) \text{ km s}^{-1}$ toward the west-southwest. This direction is roughly opposite to the motion of a handful of oxygen-rich optical filaments—presumably near-undiluted ejecta from the outer core of the progenitor—that are scattered throughout the northeast quadrant of Puppis A. Furthermore, backwards extrapolation of the motion of RX J0822-4300 indicates an origin consistent with the measured expansion center for the O-rich filaments. This completes—in at least one SNR—what is becoming almost a canonical picture for core-collapse supernovae: an asymmetric supernova explosion accompanied by recoil of the compact stellar remnant, here almost surely a neutron star.

(3) The kinetic energy associated with the transverse motion of RX J0822-4300 is $\sim 3 \times 10^{49} (d/2 \text{ kpc})^2$ ergs, only about 3% of the total of $\sim 10^{51}$ ergs expected in a typical supernova. Some 2–3 dozen O-rich knots like those now glowing optically are sufficient to balance the momentum of the neutron star.

(4) The physics of the explosion mechanism necessary to produce such a fast neutron star remains elusive, but the high kick velocity and lack of apparent pulsations from RX J0822-4300 do constrain possible models. Both these observations argue against neutrino/magnetic-field driven or electromagnetically driven mechanisms for the kick. The most likely candidate appears to be some mechanism through which hydrodynamic instabilities in the explosion lead to recoil of the compact remnant. However, the most specific such model, that of Burrows et al. (2007), is strained to explain both the high kick velocity and the apparent

absence of iron-rich ejecta from the inner core of the Puppis A progenitor.

A complete kinematic study of Puppis A, including both the oxygen knots and the stellar remnant, will be interesting and should be carried out. CCD data should enable measurement of the motions for significantly more oxygen knots than the handful used by Winkler et al. (1988), who based their study on only 11 individual knots whose motions could be measured on photographic plates. A third-epoch *Chandra* observation with the HRC-I and/or HRC-S would further cement the kinematic picture.

We have benefitted from extensive correspondence with Ralph Kraft and Almus Kenter of the *Chandra* X-ray Center at SAO regarding the *Chandra* HRC instrument, position fitting, and systematic effects. We also gratefully acknowledge valuable discussions of some statistical and computational issues attending this problem with John Emerson and Daniel Scharstein of Middlebury College, and suggestions from an anonymous referee that helped clarify our presentation. This research has been supported through the *Chandra* program by NASA grant GO4-5062X, with additional support from NSF grant AST-0307613.

REFERENCES

Burrows, A. & Hayes, J. 1996, Physical Review Letters, 76, 352

Burrows, A., Hayes, J., & Fryxell, B. A. 1995, ApJ, 450, 830

Burrows, A., Livne, E., Dessart, L., Ott, C. D., & Murphy, J. 2006, ApJ, 640, 878

—. 2007, ApJ, 655, 416

Camilo, F., Manchester, R. N., Gaensler, B. M., Lorimer, D. R., & Sarkissian, J. 2002, ApJ, 567, L71

Canizares, C. R. & Winkler, P. F. 1981, ApJ, 246, L33

Caraveo, P. A. 1993, ApJ, 415, L111+

Cash, W. 1979, ApJ, 228, 939

Chakrabarty, D., Pivovaroff, M. J., Hernquist, L. E., Heyl, J. S., & Narayan, R. 2001, ApJ, 548, 800

Cutri, R. M., Skrutskie, M. F., van Dyk, S., Beichman, C. A., Carpenter, J. M., Chester, T., Cambresy, L., Evans, T., Fowler, J., Gizis, J., Howard, E., Huchra, J., Jarrett, T., Kopan, E. L., Kirkpatrick, J. D., Light, R. M., Marsh, K. A., McCallon, H., Schneider, S., Stiening, R., Sykes, M., Weinberg, M., Wheaton, W. A., Wheelock, S., & Zacarias, N. 2003, 2MASS All Sky Catalog of point sources. (The IRSA 2MASS All-Sky Point Source Catalog, NASA/IPAC Infrared Science Archive. <http://irsa.ipac.caltech.edu/applications/Gator/>)

Dodson, R., Legge, D., Reynolds, J. E., & McCulloch, P. M. 2003, ApJ, 596, 1137

Fesen, R. A. 2001, ApJS, 133, 161

Frail, D. A., Goss, W. M., & Whiteoak, J. B. Z. 1994, ApJ, 437, 781

Gaensler, B. M. 2000, in ASP Conf. Ser. 202: IAU Colloq. 177: Pulsar Astronomy - 2000 and Beyond, ed. M. Kramer, N. Wex, & R. Wielebinski, 703–+

Gaensler, B. M., Bock, D. C.-J., & Stappers, B. W. 2000, ApJ, 537, L35

Hughes, J. P., Slane, P. O., Burrows, D. N., Garmire, G., Nousek, J. A., Olbert, C. M., & Keohane, J. W. 2001, ApJ, 559, L153

Hui, C. Y. & Becker, W. 2006a, A&A, 457, L33 (HB06a)

—. 2006b, A&A, 454, 543

Hwang, U., Holt, S. S., & Petre, R. 2000, ApJ, 537, L119

Hwang, U., Laming, J. M., Badenes, C., Berendse, F., Blondin, J., Cioffi, D., DeLaney, T., Dewey, D., Fesen, R., Flanagan, K. A., Fryer, C. L., Ghavamian, P., Hughes, J. P., Morse, J. A., Plucinsky, P. P., Petre, R., Pohl, M., Rudnick, L., Sankrit, R., Slane, P. O., Smith, R. K., Vink, J., & Warren, J. S. 2004, ApJ, 615, L117

Hwang, U., Petre, R., Flanagan, K., & Figueroa-Feliciano, E. 2007, Prog. Theoret. Phys. Suppl.

Johnston, S., Hobbs, G., Vigeland, S., Kramer, M., Weisberg, J. M., & Lyne, A. G. 2005, MNRAS, 364, 1397

Kirshner, R. P., Morse, J. A., Winkler, P. F., & Blair, W. P. 1989, ApJ, 342, 260

Lai, D. 2001, LNP Vol. 578: Physics of Neutron Star Interiors, 578, 424

Laming, J. M., Hwang, U., Radics, B., Lekli, G., & Takács, E. 2006, ApJ, 644, 260

Lawrence, S. S., MacAlpine, G. M., Uomoto, A., Woodgate, B. E., Brown, L. W., Oliversen, R. J., Lowenthal, J. D., & Liu, C. 1995, AJ, 109, 2635

Manchester, R. N. 2001, in AIP Conf. Proc. 565: Young Supernova Remnants, ed. S. S. Holt & U. Hwang, 305–314

Migliazzo, J. M., Gaensler, B. M., Backer, D. C., Stappers, B. W., van der Swaluw, E., & Strom, R. G. 2002, ApJ, 567, L141

Morse, J. A., Winkler, P. F., & Kirshner, R. P. 1995, AJ, 109, 2104

Murray, S. S., Ransom, S. M., Juda, M., Hwang, U., & Holt, S. S. 2002, ApJ, 566, 1039

Ng, C.-Y. & Romani, R. W. 2004, ApJ, 601, 479

Pavlov, G. G., Sanwal, D., Garmire, G. P., & Zavlin, V. E. 2002, in ASP Conf. Ser. 271: Neutron Stars in Supernova Remnants, ed. P. O. Slane & B. M. Gaensler, 247–+

Petre, R., Becker, C. M., & Winkler, P. F. 1996, ApJ, 465, L43+

Press, W. H., Flannery, B. P., Teukolsky, S. A., & Vetterling, W. T. 1992, Numerical Recipes, the Art of Scientific Computing, second edition (Cambridge: Cambridge U. Press), 684–694

Reed, J. E., Hester, J. J., Fabian, A. C., & Winkler, P. F. 1995, ApJ, 440, 706

Reynoso, E. M., Dubner, G. M., Goss, W. M., & Arnal, E. M. 1995, AJ, 110, 318

Reynoso, E. M., Green, A. J., Johnston, S., Dubner, G. M., Giacani, E. B., & Goss, W. M. 2003, MNRAS, 345, 671

Sakhibov, F. K. & Smirnov, M. A. 1983, Soviet Astronomy, 27, 395

Scheck, L., Kifonidis, K., Janka, H.-T., & Müller, E. 2006, A&A, 457, 963

Scheck, L., Plewa, T., Janka, H.-T., Kifonidis, K., & Müller, E. 2004, Physical Review Letters, 92, 011103

Seward, F. D., Harnden, Jr., F. R., & Helfand, D. J. 1984, ApJ, 287, L19

Spruit, H. C. & Phinney, E. S. 1998, Nature, 393, 139

Tamura, K., Tsunemi, H., & Petre, R. 1994, in New Horizon of X-Ray Astronomy. First Results from ASCA, ed. F. Makino & T. Ohashi, 487–+

Tananbaum, H. 1999, IAU Circ., 7246, 1

Thorstensen, J. R., Fesen, R. A., & van den Bergh, S. 2001, AJ, 122, 297

Wang, C., Lai, D., & Han, J. L. 2006, ApJ, 639, 1007

Willingale, R., Bleeker, J. A. M., van der Heyden, K. J., & Kaastra, J. S. 2003, A&A, 398, 1021

Winkler, P. F. & Kirshner, R. P. 1985, ApJ, 299, 981

Winkler, P. F., Tuttle, J. H., Kirshner, R. P., & Irwin, M. J. 1988, in IAU Colloq. 101: Supernova Remnants and the Interstellar Medium, ed. R. S. Roger & T. L. Landecker, 65–+

Zacharias, N., Urban, S. E., Zacharias, M. I., Wycoff, G. L., Hall, D. M., Germain, M. E., Holdenried, E. R., & Winter, L. 2003, VizieR Online Data Catalog, 1289, 0

Table 1. *Chandra* HRC Observations of RXJ0822–4300.

Obs ID	Sequence No	Detector	Date	Exposure (ks)
749	500045	HRC-I	1999 Dec 21-22	15.9
1851	500122	HRC-S	2001 Jan 25	19.5
4612	500437	HRC-I	2005 Apr 25	33.1

Table 2. Astrometric Reference Stars from UCAC2 Catalog^a

Designation		Position		Pos'n Uncertainty		Proper Motion		Distance from NS ^b
Short	2UCAC No	RA (2000.)	Dec (2000.)	σ_{RA} (mas)	σ_{Dec} (mas)	μ_{RA} (mas yr $^{-1}$)	μ_{Dec} (mas yr $^{-1}$)	($'$)
A	13302738	8 ^h 21 ^m 46 ^s .294	-43°02'03".64	15	15	-16.0 ± 5.2	-1.7 ± 5.2	2.7
C	13302743	8 21 48.875	-43 01 28.34	15	15	-65.5 ± 4.7	-7.0 ± 4.7	2.0
B	13520024	8 22 24.004	-42 57 59.36	24	15	- 4.2 ± 5.2	14.8 ± 5.2	5.4

^aZacharias et al. (2003)

^bAngular separation from the central neutron star RXJ0822-4300.

Table 3. Properties of *Chandra* X-ray Sources and Positions for Optical Counterparts

Obs ID	Epoch	Source	X-ray Position ^{a,b}		Count Rate counts ks ⁻¹	UCAC2 Position ^c	
			RA (2000.)	Dec (2000.)		RA (2000.)	Dec (2000.)
749	1999.98	NS	8 ^h 21 ^m 57 ^s 410(01)	-43°00'16.66(01)	195.5		
		A	8 21 46.284(10)	-43 02 03.13(24)	3.0	8 ^h 21 ^m 46 ^s .294	-43°02'03.64
		B	8 22 23.915(24)	-42 57 59.48(21)	6.7	8 22 24.004	-42 57 59.36
1851	2001.07	NS	8 21 57.393(01)	-43 00 16.68(01)	315.4		
		A	8 21 46.331(06)	-43 02 03.41(08)	4.9	8 21 46.292	-43 02 03.64
		B	8 22 23.871(13)	-42 57 59.04(13)	10.0	8 22 24.003	-42 57 59.34
4612	2005.32	NS	8 21 57.364(01)	-43 00 16.99(01)	209.0		
		A	8 21 46.296(06)	-43 02 03.45(04)	3.5	8 21 46.286	-43 02 03.65
		B	8 22 24.005(09)	-42 57 59.12(28)	5.4	8 22 24.002	-42 57 59.28

^aPosition determined from fit of appropriate PSFs to HRC data (see text).

^bUncertainty (1σ) in last two digits in parentheses.

^cZacharias et al. (2003); corrected for proper motion.

Table 4. Position and Proper Motion Measurements for RXJ0822-4300.^a

Obs IDs	Baseline (yr)	Method	Displacement (mas)	Proper Motion (mas yr ⁻¹)	Position Angle ^b
749-4612	5.34	shift only ^c	752 ± 131	141 ± 24	250° ± 14°
749-4612	5.34	rot-scale ^d	990 ± 149	185 ± 28	254° ± 16°
1851-4612	4.25	rot-scale ^d	716 ± 100	168 ± 23	240° ± 13°
Mean ^e				165 ± 25	248° ± 14°

^aCorrected position for RX J0822-4300 in 2005 April observation: RA(2000.) = 8^h21^m57^s.355, Dec(2000.) = -43°00'17".17.

^bMeasured north through east.

^cSmall RA and Dec shifts alone are used to align stars A and B in the two images (§3.2).

^dImages at all three epochs are placed on a common absolute frame through a linear transformation that allows rotation and a uniform scale change in addition to translations to align stars A and B with their optical positions (§3.3).

^eMean is the unweighted average of all three measurements.

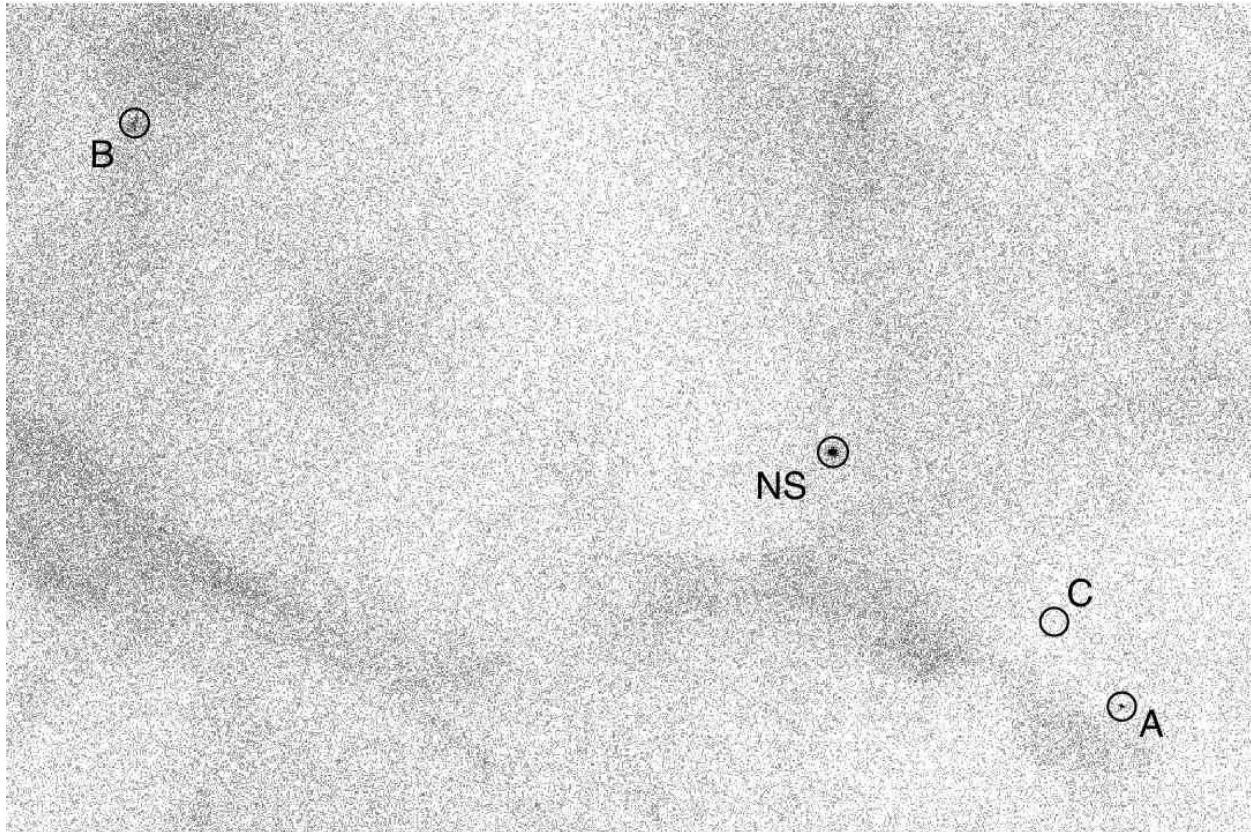


Fig. 1.— The 2005 epoch *Chandra* HRC-I image with sources marked by 12'' diameter circles. NS is the presumed neutron star, A and B correspond to fiducial stars used in our analysis, and C marks the position of a third star detected at only the $\sim 2\sigma$ level in 2005 (see also Fig. 2). The field measures 8.6×5.7 and is oriented north up, east left.

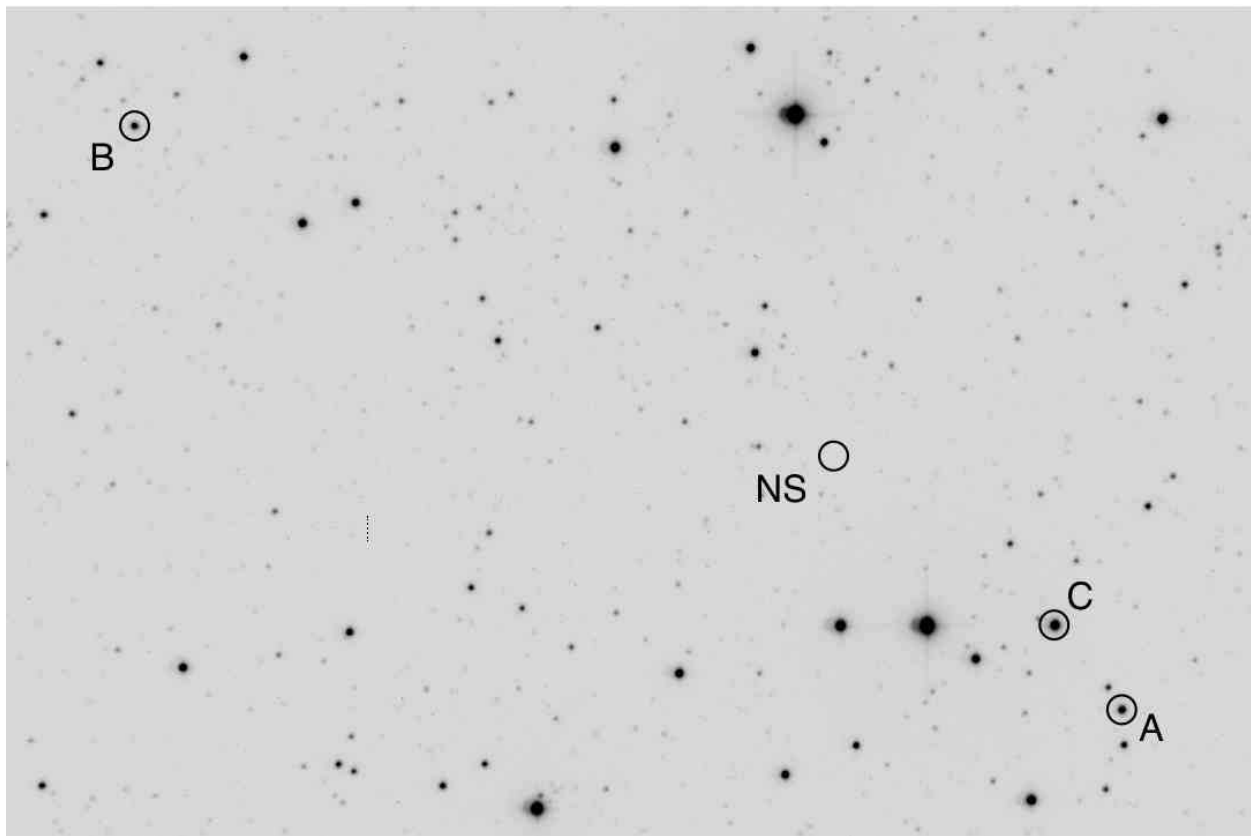


Fig. 2.— Optical image of the identical field as Figs. 1 and 4, with the astrometric reference stars marked (the same overlay as Fig. 1). The image was obtained at the CTIO 0.9 m telescope using a narrow-band red continuum filter.

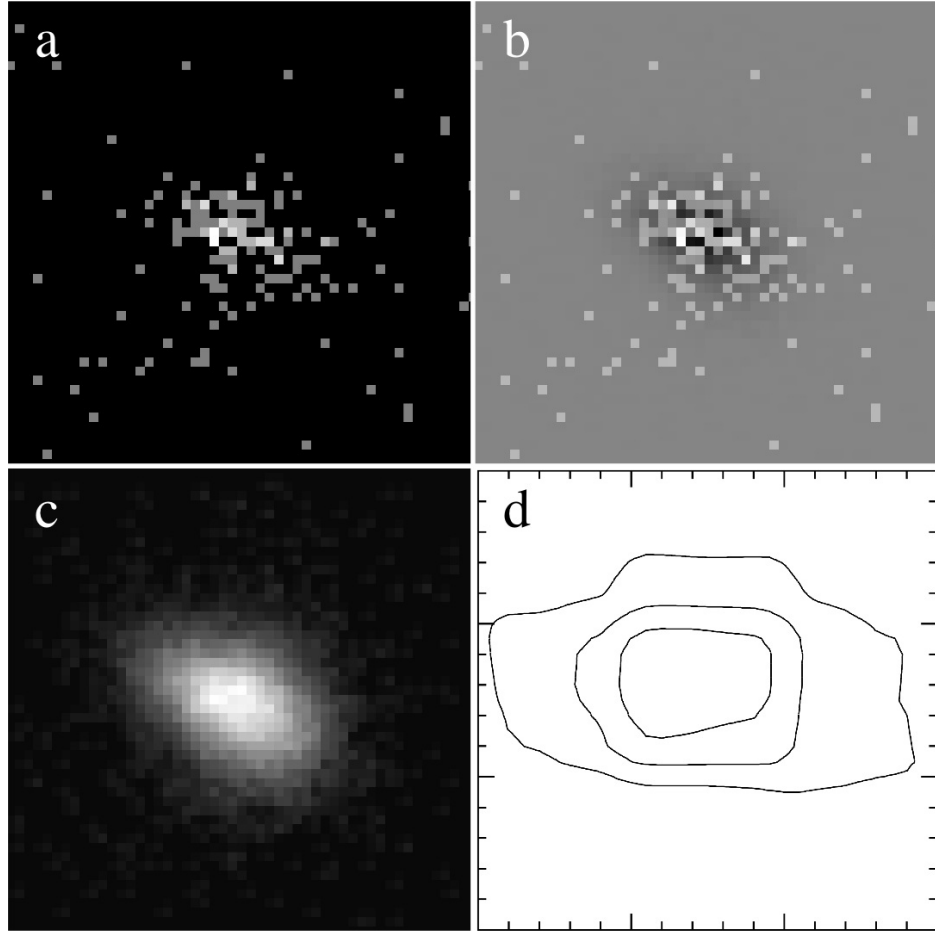


Fig. 3.— Example of a typical source position fit—this for star A at epoch 2005 (Obs ID 4612): (a) The HRC-I data displayed at full resolution; the small squares are individual HRC pixels, $0''.1318$ square, and the field shown here (and in panels b and c) is 50 pixels = $6''.6$ square. (c) The PSF as simulated using ChaRT and MARX for a source with the same off-axis angle and azimuth as star A in this observation. (b) The difference between the actual data (panel a) and the best-fit source model after convolution with the PSF in panel c. The position, intensity, and constant background level have been adjusted in the fit. (d) A map of confidence contours for the position fit; the major ticks represent 1 HRC pixel, and the full field here is only 3 pixels = $0''.40$ square. The Cash statistic has been computed at each (x, y) point in a fine grid, with the intensity and background readjusted to give the minimum value at that point. The contours correspond to 1, 2, and 3σ (increments of 2.3, 6.2, and 11.8 above the minimum statistic value). The contours are not circular, but the 1σ uncertainty in any direction is $\lesssim \pm 0.5$ pixels $\approx 0''.065$. Similar fits were carried out for the NS and for stars A and B at all three epochs, to obtain the values given in Table 3.

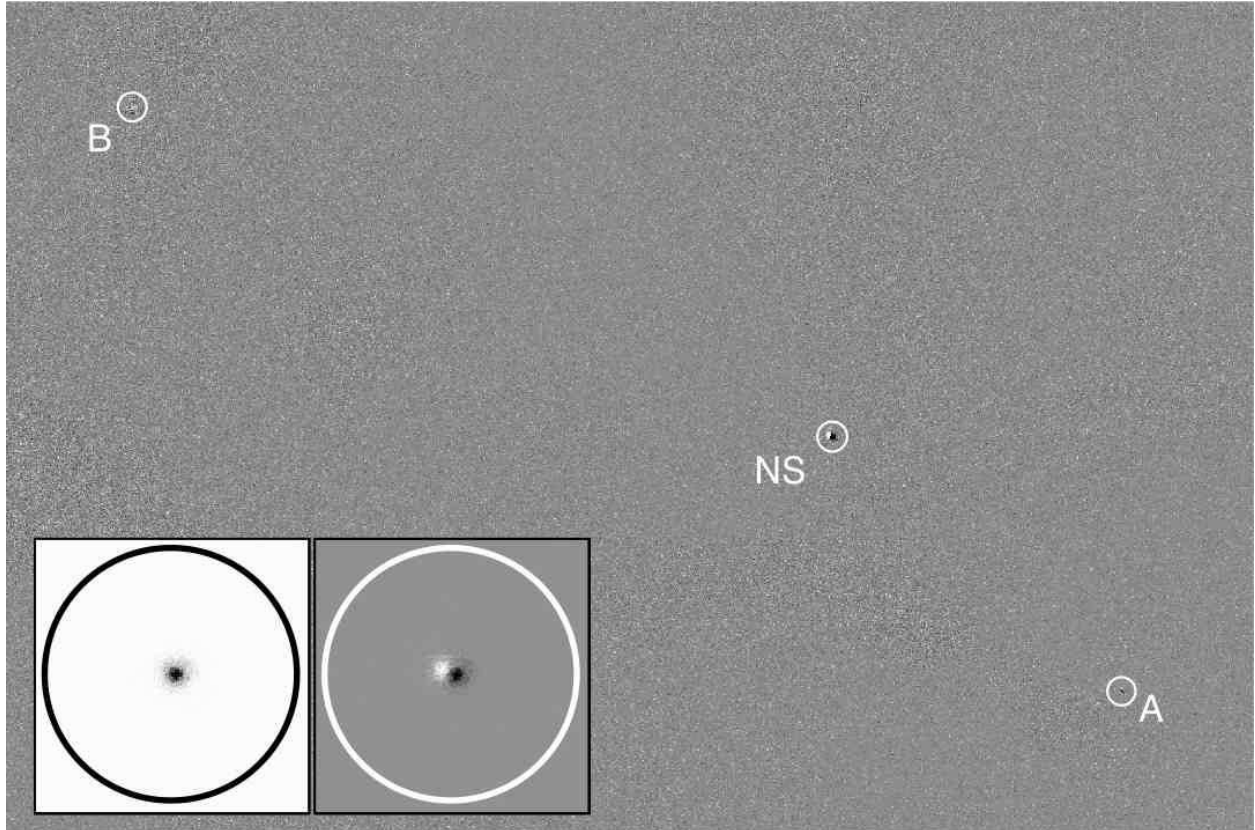


Fig. 4.— Difference between the 1999 epoch (events white) and 2005 epoch (events black) HRC-I images, registered and scaled by the exposure time. The field is the same as in Figs. 1 and 2. The reference stars A and B largely disappear in the difference image, but RX J0822–4300 shows a noticeable displacement between the two epochs. This motion is more evident in the detailed view shown in the inset: (*left*) the 2005 epoch image alone, and (*right*) the difference image. The images are the same as those shown in Figs. 1 and 4, but the stretch has been changed to emphasize the narrow ($\sim 0''.5$) point-spread function. The circles in the inset are $12''$ in diameter, the same as in the full image and in Fig. 1. Proper motion toward the west-southwest is apparent, with a displacement roughly twice the width of the PSF.

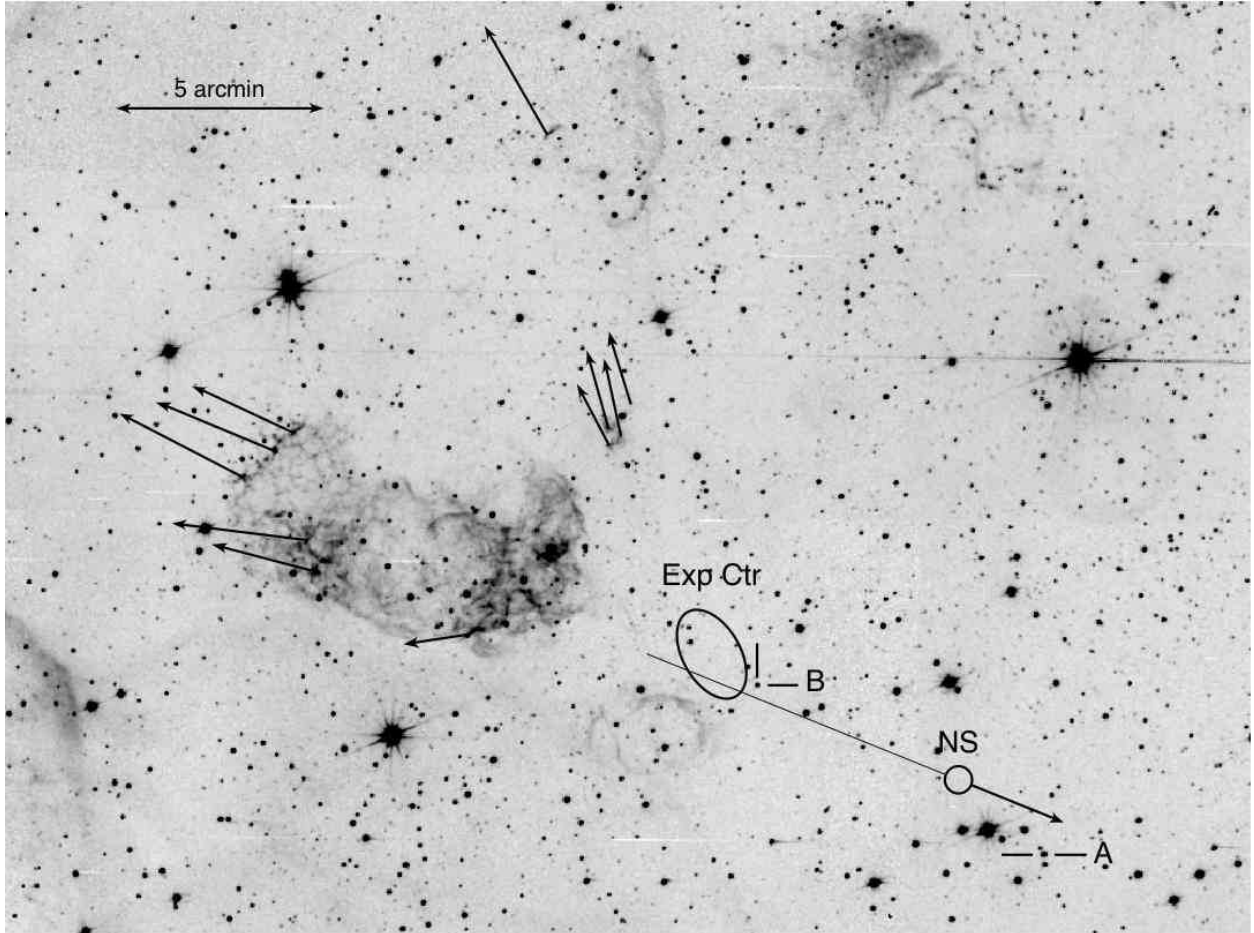


Fig. 5.— Optical image of the central region of Puppis A in [O III] λ 5007, showing proper motions of the O-rich filaments and RX J0822–4300. The arrows indicate proper-motion vectors for ~ 1000 yr, and the ellipse shows the 90%-confidence contour for the expansion center. (This is a wider-field version of Fig. 1 from Winkler et al. 1988, overlaid on a more recent CCD image.) The circle marked NS shows the present position for the presumed neutron star, RX J0822–4300, and the attached vector indicates its motion over 1000 yr at the rate we have measured. Backwards extrapolation of its present motion (lighter line) passes well within the error ellipse for the expansion center of the O-rich filaments.